SCIENCE CHINA Materials ARTICLES

mater.scichina.com link.springer.com

Published online 18 September 2019 | https://doi.org/10.1007/s40843-019-9586-x
Sci China Mater 2020, 63(2): 207–215

A low-temperature TiO_2/SnO_2 electron transport layer for high-performance planar perovskite solar cells

Nan Li[1,2], Jin Yan[1,2], Yuqian Ai[1], Ershuai Jiang[1,2], Liujin Lin[1], Chunhui Shou[3], Baojie Yan[1], Jiang Sheng[1*] and Jichun Ye[1,2*]

ABSTRACT **Conventional titanium oxide (TiO_2) as an electron transport layer (ETL) in hybrid organic-inorganic perovskite solar cells (PSCs) requires a sintering process at a high temperature to crystalize, which is not suitable for flexible PSCs and tandem solar cells with their low-temperature-processed bottom cell. Here, we introduce a low-temperature solution method to deposit a TiO_2/tin oxide (SnO_2) bilayer towards an efficient ETL. From the systematic measurements of optical and electronic properties, we demonstrate that the TiO_2/SnO_2 ETL has an enhanced charge extraction ability and a suppressed carrier recombination at the ETL/perovskite interface, both of which are beneficial to photo-generated carrier separation and transport. As a result, PSCs with TiO_2/SnO_2 bilayer ETLs present higher photovoltaic performance of the baseline cells compared with their TiO_2 and SnO_2 single-layer ETL counterparts. The champion PSC has a power conversion efficiency (PCE) of 19.11% with an open-circuit voltage (V_{oc}) of 1.15 V, a short-circuit current density (J_{sc}) of 22.77 mA cm^{-2}, and a fill factor (FF) of 72.38%. Additionally, due to the suitable band alignment of the TiO_2/SnO_2 ETL in the device, a high V_{oc} of 1.18 V is achieved. It has been proven that the TiO_2/SnO_2 bilayer is a promising alternative ETL for high efficiency PSCs.**

Keywords: perovskite solar cell, electron transport layer, TiO_2/SnO_2, low temperature, energy band alignment

INTRODUCTION

The research and development of hybrid organic-inorganic perovskite solar cells (PSCs) has increased dramatically in the past decade, with an amazing power conversion efficiency (PCE) improvement from 3.8% to more than 23% [1–4]. The advanced perovskite materials have been successfully applied in the field of solar cells [5] thanks to their numerous advantages of high light absorption efficiency in the visible wavelength region, long carrier diffusion length, tunable bandgap, and high tolerance for defect states. They are thus considered to be one of the most promising next-generation solar energy materials [6–9].

Generally, in order to improve the electron extraction, a mesoporous TiO_2 electron transport layer (ETL) is normally used in high-performance PSCs to increase the contact area of TiO_2 and the perovskite [10–11]. It is usually prepared by using a spray pyrolysis technique or spin-coating with the sol-gel method, followed by a high-temperature (>450°C) sintering step, which is critical for crystallizing the TiO_2 layer to improve the electrical conductivity [12]. However, the high-temperature process is usually incompatible with flexible substrates and monolithic tandem systems with a low-temperature-processed bottom cell. Additionally, compared with mesoporous PSCs, planar heterojunction structure (PHJ) PSCs are easier to fabricate and have a lower cost. This has recently rendered PHJ PSCs as prospective commercial candidates [13–17].

Although low-temperature processes for fabricating TiO_2 films have been reported, such as chemical bath deposition, atomic layer deposition and the electrodeposited method, the performances of PSCs based on these methods are still too low [18–19]. The TiO_2 ETLs derived from the low-temperature process can result in the inferior PCE and the hysteresis of PSCs due to their poor crystallinity, low electrical conductivity, and high density of trap states [20–21]. To solve these problems, doping and surface modifications have been widely researched in recent years. Hu *et al.* [22] reported that upon applying NH_2-TiO_2 nanoparticles as a novel ETL in the

[1] Ningbo Institute of Material Technology and Engineering, Chinese Academy of Sciences, Ningbo 315201, China
[2] University of Chinese Academy of Sciences, Beijing 100049, China
[3] Zhejiang Energy Group R&D, Hangzhou 310003, China
* Corresponding authors (emails: shengjiang@nimte.ac.cn (Sheng J); jichun.ye@nimte.ac.cn (Ye J))

low-temperature process, the regular-structure PSCs exhibited a significant PCE improvement to over 21%. Liu and coworkers [23] introduced zinc ions into a compact TiO_2 lattice by a simple low-temperature solution process, which improved the interfacial carrier extraction between the ETL and perovskite, obtaining a PCE of 19.04% with 4.5% Zn-doped ETL PSCs. However, the TiO_2/perovskite interface still has many trap states responsible for severe recombination loss, especially when exposed to UV light, leading to strong hysteresis behaviors [24]. To pursue high-performance and nonhysteretic PSCs, many passivation methods, such as applying a fullerene self-assembled monolayer or [6,6]-phenyl-C61-isomethyl butyrate (PCBM) to the TiO_2 surface, as well as chlorine-capped TiO_2 nanocrystal films, have been reported [25–27]. However, these methods are complex and expensive, so low-cost and high quality ETLs still urgently need to be explored for high-efficiency and stable PSCs, as well as for further possible commercialization.

On the other hand, tin oxide (SnO_2) is a promising alternative for high-performance PSCs in low-temperature preparations due to its low cost and high quality (high charge extraction efficiency, high carrier mobility and wide band gap) [28–30]. SnO_2 can remarkably reduce or even eliminate the hysteresis phenomenon of planar PSCs. Therefore, combining the advantages of TiO_2 and SnO_2 as the double layer ETL is a good choice to improve the electron extraction and transport properties and rearrange the band alignment for high electron collection efficiency. This topic has also been reported in recent years. For instance, Song *et al.* [31] reported a 21.1% PCE of the planar PSCs using a TiO_2/SnO_2 bilayer ETL. Tavakoli *et al.* [32] employed an amorphous SnO_2 on the top of a compact TiO_2 layer as the ETL, achieving a PCE of 21.4%. However, the high-temperature process was still employed to improve the film quality, limiting its application in flexible PSCs and tandem solar cells.

In this work, a TiO_2/SnO_2 bilayer ETL is proposed for planar PSCs to be fabricated at a low temperature (≤150°C). The band alignment is properly tuned to improve the open-circuit voltage (V_{oc}) of the PSCs. By adjusting the bottom of the conduction band edge of the ETL to reduce the conduction band edge offset with that of the perovskite layer, the barrier height is decreased for the effective electron extraction from the perovskite and highly efficient transport to the electrode. Moreover, by inserting an SnO_2 layer to passivate the defects at the TiO_2 surface, the hysteresis of the PSCs can be amended, and the stability can also be improved against prolonged illumination. As expected, the PSCs with bilayer ETL show a noticeable improvement in V_{oc} and the fill factor (FF), demonstrating that this bilayer ETL is suitable in the low-temperature manufacturing process for high-performance PSCs.

EXPERIMENTAL SECTION

Materials

The indium tin oxide (ITO) glass substrates were supplied by the CSG Holding Co., Ltd. The SnO_2 colloid precursor was purchased from Alfa Aesar. Formamidinium iodide (FAI; 99.5%), methylammonium iodide (MAI; 99.5%) and spiro-OMeTAD (99.5%) were obtained from Xi'an P-OLED Corp. The PbI_2 and $PbBr_2$ were received from Sigma-Aldrich. All other reagents were all purchased from Aladdin.

Synthesis

The TiO_2 nanoparticle solution was synthesized as follows: 470 μL tetrabutyl titanate was added dropwise into 2.5 mL of ethanol with 111 μL of nitric acid under mild stirring of 500 rpm. After 2 h of stirring, 127 μL of deionized water was put into the mix solvent for the hydrolysis of tetrabutyl titanate. This reaction continued for 1 h. Finally, the isopropanol was added into the resulting solution to form the 0.127 mol L^{-1} TiO_2 solution. This transparent solution of TiO_2 was prepared for spin-coating, without any washing, centrifugation and dispersing. The SnO_2 precursor (15% in H_2O colloidal dispersion) was diluted by water. To obtain the perovskite precursor, 24.4 mg methylammonium bromide (MABr), 85.4 mg $PbBr_2$, 214.5 mg FAI, and 607.9 mg PbI_2 were dissolved in 0.33 mL of dimethyl sulfoxide (DMSO) and 0.67 mL *N*,*N*-dimethylformamide (DMF) mixture, and then stirred at 60°C for 12 h. The hole transport layer (HTL) solution contained 72.3 mg of spiro-OMeTAD, 28.8 μL of 4-*tert*-butyl pyridine (TBP), 17.5 μL of a lithium bis(trifluoromethane-sulfonyl)imide (Li-TFSI) solution (520 mg of Li-TSFI in 1 mL of acetonitrile), and 8 μL of a cobalt bis(trifluoromethanesulfonyl)imide (Co-TFSI) solution (360 mg of Co-TSFI in 1 mL of acetonitrile) in 1 mL of chlorobenzene.

Device fabrication

The patterned ITO-coated glass substrates were ultrasonically cleaned by acetone, isopropanol, and deionized water, and then dried immediately by a flow of pure nitrogen. Then, the substrates were further treated by UV-ozone for 15 min for the subsequent deposition of films. The TiO_2 and SnO_2 ETLs were both prepared by spin-

coating with their nanoparticle precursor solutions on the ITO glass at 5000 rpm for 30 s in ambient air, and then annealed on a hot plate at 140 and 150°C for 30 min, respectively. The TiO_2/SnO_2 bilayer ETL was also obtained by spin-coating the SnO_2 precursor solution directly onto the pre-prepared TiO_2 samples using the same process as the monolayer film deposition. Then, three kinds of ETLs, TiO_2, SnO_2 and TiO_2/SnO_2, were ready for depositing the perovskite absorber and HTL. The 20 μL perovskite precursor was spin-coated at 4500 rpm for 40 s, during which 220 μL of chlorobenzene was dropped rapidly (20 s) prior to the ending. Then, this wet perovskite film was baked at 140°C for 10 min for crystallization. The HTL solution was spin-coated on the perovskite layer at 4500 rpm for 30 s. Finally, an 80 nm sliver electrode was evaporated on the spiro-OMeTAD layer for the integrated PSC.

Characterizations

The photovoltaic performance of PSCs was determined using a solar simulator (Oriel, Sol3A) with a Xe-arc lamp under Air-mass 1.5 illumination (100 mW cm^{-2}). A standard silicon solar cell from Newport Corporation was used to calibrate the illumination intensity. All of the PSCs were exposed to ambient air and masked by a black metal mask with an active area of 0.1 cm^2 during the testing. For the electrochemical impedance spectroscopy (EIS) measurement, the PSCs were tested in a frequency range between 1 MHz and 10 Hz. The external quantum efficiency (EQE) spectra were recorded with a commercial apparatus (Newport 2936-cpowermeter) based on a 300 W xenon lamp. The morphology images of the ETL films were obtained by the scanning probe microscope (SPM, Veeco, Dimension 3100), while the morphology of the perovskite surface on the three different ETL films (TiO_2, SnO_2 and TiO_2/SnO_2) and the cross section of the device were characterized by the scanning electron microscope (SEM, Thermo Scientific, Verios G4 UC). The transmittance spectra of the samples were acquired by using Ultraviolet-visible spectroscopy (UV/Vis, Perkin-Elmer, Lambda 950). A HORIBA FL3-111 fluorescence spectrometer was employed for the steady-state and time-resolved photoluminescence. The excitation wavelength was 460 nm and the PL spectra were recorded in the wavelength range of 300–850 nm. The thickness of the TiO_2 and SnO_2 layer was analyzed *via* ellipsometry (Alpha-SE). The ultraviolet photoelectron spectroscopy (UPS, Axis Ultra DLD, Kratos Analytical Ltd, UK) was used to measure the work function of different ETLs.

RESULTS AND DISCUSSION

The structural schematic of the PSC with a TiO_2/SnO_2 bilayer ETL is shown in Fig. 1a, with the corresponding cross-sectional SEM image shown in Fig. 1b. Clearly, the device is composed of a ~200 nm ITO layer, a ~37 nm TiO_2/SnO_2 bilayer ETL, a ~520 nm perovskite absorption layer, a ~140 nm spiro-OMeTAD HTL, and a ~80 nm Ag electrode film. The cross-sectional SEM images of the PSCs based on TiO_2 and SnO_2 ETLs are shown in Fig. S1, of which the optimum thicknesses are 20 and 28 nm, respectively. Fig. 1c presents the current-voltage (*J-V*) curves scanned in forward and reverse directions of the champion PSC based on the TiO_2/SnO_2 bilayer ETL. The top-view SEM images of the perovskite films deposited onto the TiO_2/SnO_2 bilayer by an antisolvent method are displayed in Fig. 1d, exhibiting a more uniform surface and a larger grain size than those on the TiO_2 and SnO_2 ETLs demonstrated in Fig. S2.

To understand the charge transfer properties of different ETLs, steady and time-resolved photoluminescence (PL and TRPL) spectroscopies were investigated. As shown in Fig. 2a, the perovskite film deposited onto the TiO_2/SnO_2 bilayer exhibits a much stronger quenching effect than those on the monolayer TiO_2 and SnO_2 films, suggesting a more efficient charge transfer from the perovskite to the TiO_2/SnO_2 ETL, due to the decreasing defects at the ETL/perovskite interface. Similarly, Fig. 2b displays that the perovskite film on TiO_2/SnO_2 ETL accelerates the PL decay in comparison with the monolayer samples. Table S1 shows the lifetime and corresponding amplitudes fitted by using a biexponential decay function. Usually the fast decay component (τ_1) is attributed to the quenching of charge carriers at the interface of the ETL and perovskite, and the slow decay component (τ_2) reflects the nonradiative recombination of carriers through the recombination center of the perovskite layer [33]. Both the fast and slow decay components of the perovskite film on the TiO_2/SnO_2 ETL are the lowest among the three samples, which are 13 and 369 ns, respectively. This indicates that the TiO_2/SnO_2 ETL has better electron transfer and extraction properties, which can be attributed to less electron accumulation at the ETL/perovskite interface and a suitable conduction band alignment between the TiO_2/SnO_2 ETL and perovskite.

As seen in Fig. 3, the film surface morphologies of the three different ETLs deposited on the ITO glass were monitored by a SPM. The atomic force microscopy (AFM) images (5 × 5 μm^2 scan area) reveal that the values of the root-mean-square roughness (RMS) of the TiO_2, SnO_2, and TiO_2/SnO_2 films are 2.44, 1.83, and 1.67 nm,

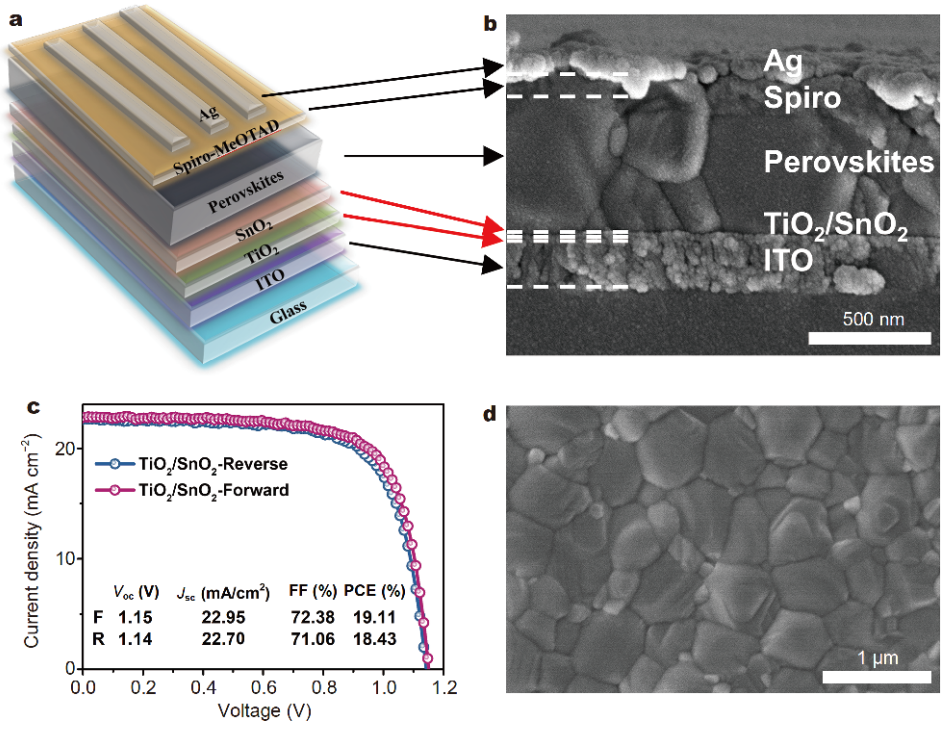

Figure 1 The schematic image (a) and cross-sectional SEM image of the PSC based on TiO_2/SnO_2 bilayer ETL (b), the *J-V* curves (c) of the champion PSC under forward and reverse sweep, labeled as F and R respectively, and top view SEM image (d) of the perovskite film deposited on TiO_2/SnO_2 bilayer.

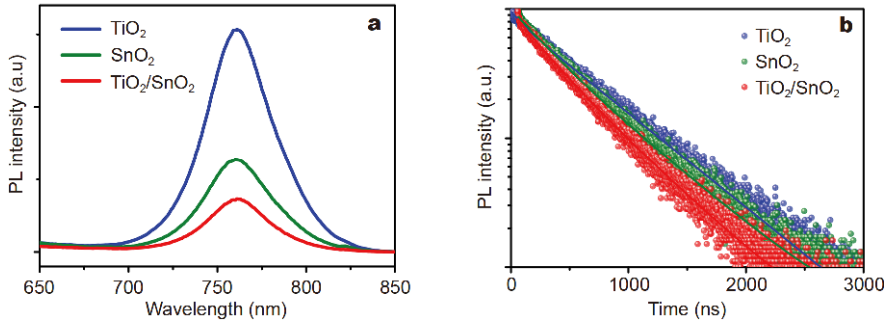

Figure 2 PL spectra (a) and TRPL curves (b) of perovskite film deposited on different ETLs: TiO_2, SnO_2, and TiO_2/SnO_2.

respectively. The lower roughness of the TiO_2/SnO_2 films is a vital figure-of-merit for the PSCs, leading to a better quality of the perovskite films and the crystal growth [34]. Additionally, both of the single TiO_2 and SnO_2 films might cause pinholes in large scale, but the TiO_2/SnO_2 bilayer can fully cover the ITO substrate, which is important for reducing the current leakages at the interface of the electrode in the device.

To understand the reason for the performance improvement, an UPS measurement was used to determine the work function and valence bands of the different ETLs. Fig. 3d shows the calculated Fermi level (E_f) and valence band (E_v) values of the TiO_2, SnO_2, and TiO_2/SnO_2. As exhibited in the UV-vis spectra in Fig. S3, the optical bandgaps of TiO_2, SnO_2, and TiO_2/SnO_2 are 3.87, 4.13 and 4.13 eV, respectively. By associating the UV-vis and UPS data, the valence and conduction bands of TiO_2, SnO_2, and TiO_2/SnO_2 ETLs are figured out. As shown in Fig. 3e, the conduction bands of TiO_2, SnO_2, and TiO_2/SnO_2 ETLs are approximately 4.45, 4.03, and 3.94 eV, respectively, and the values for the perovskite are referenced in [35]. The decrease in the conduction band values

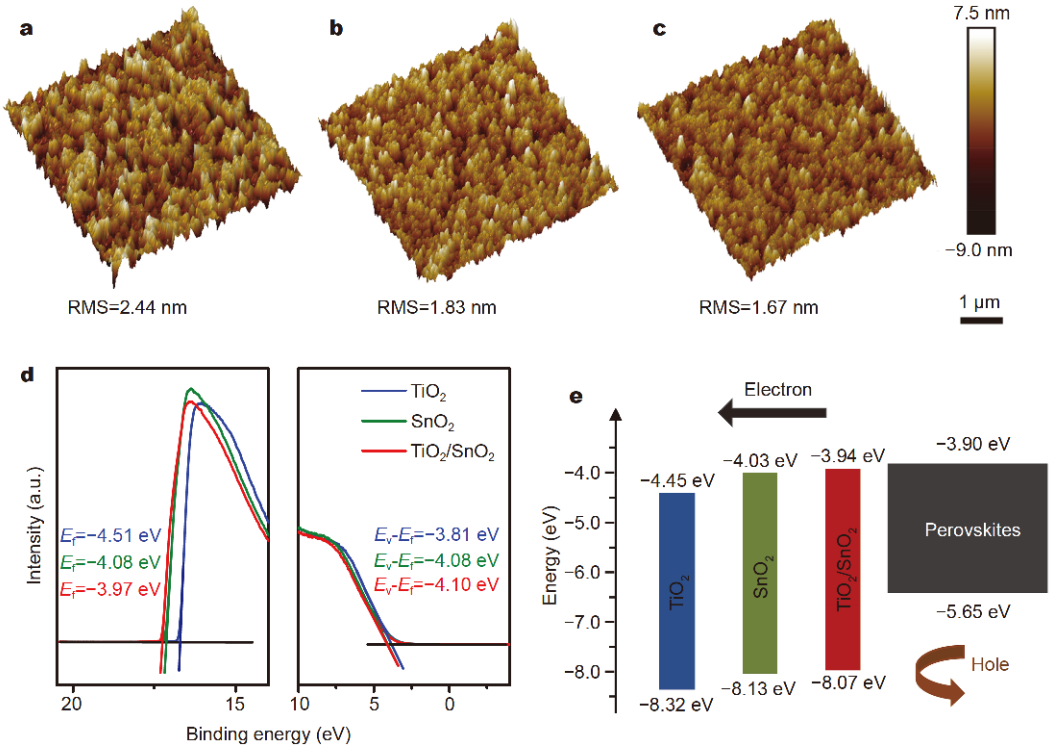

Figure 3 3D-AFM images (a–c) of ITO/TiO_2, ITO/SnO_2 and ITO/TiO_2/SnO_2 films, respectively, (d) UPS measurements of above samples, (e) the diagram of band alignment for different ETLs: TiO_2, SnO_2, and TiO_2/SnO_2.

means that the energy offset between the ETLs and perovskite is narrowed, which is conducive to enhancing V_{oc} [32].

To find the optimum ETL fabrication process, we further investigated the influence of the thickness and annealing temperature on the photovoltaic performance of the PSCs. From Fig. S5, we can deduce that the monolayer TiO_2 PSC presents the best performance with an annealing temperature of 140°C. Moreover, for the TiO_2/SnO_2 bilayer, the TiO_2 film was fixed at 12 nm to ensure sufficient transmittance, so measurements with different SnO_2 film thicknesses (20, 25 and 30 nm) were performed. The obtained photovoltaics results reveal that the performance of the TiO_2/SnO_2 PSC is sensitive to the annealing temperature and the thickness of the SnO_2 film. As shown in Fig. S6, the 25 nm SnO_2 film is the optimized thickness to achieve the maximum efficiency. These experiments also suggest that the TiO_2/SnO_2 bilayer ETL is better than the TiO_2 and SnO_2 monolayer ETLs.

To discuss the differences of the photovoltaic performance for various ETLs, we prepared 45 pieces of PSCs of every condition to analyze the results under light illumination. Fig. 4a shows the *J-V* curves of the champion devices with different ETLs scanned in the forward and reverse directions under an AM1.5 solar simulator. The statistical data of V_{oc}, the short circuit current density (J_{sc}), FF and PCE are summarized in Table 1. The TiO_2/SnO_2 PSCs exhibit less hysteresis compared with the monolayer TiO_2 or SnO_2 PSCs. Generally, charges or ions accumulation and a charge transfer imbalance at the interface of the ETL/perovskite are the prime reasons for the hysteresis in PSCs. It is expected that revising the band alignment and improving the electron extraction of the TiO_2/SnO_2 bilayer ETL could reduce the hysteresis in the PSCs. As expected, the TiO_2/SnO_2 devices show a champion PCE of 19.11%, with a V_{oc} of 1.15 V, a J_{sc} of 22.77 mA cm^{-2}, and an FF of 72.38%. In this regard, the SnO_2 and TiO_2 devices exhibit a PCE of 17.40% and 14.76%, respectively. Fig. 4b shows the EQE data of PSCs with the various ETLs, and the integrated J_{sc} values of the devices based on the TiO_2, SnO_2, and TiO_2/SnO_2 ETLs are 21.75, 21.54 and 19.23 mA cm^{-2}, respectively, which are also in good accord with the trend of J_{sc} under the simulated light. The electrical conductivity of SnO_2 is much better than the amorphous TiO_2. Thus, the J_{sc} is improved significantly for SnO_2 and TiO_2/SnO_2 PSCs, compared with that of TiO_2 PSC. Fig. 4c–f provide the PCE box-chart and the other photovoltaic parameters of the *J-V*

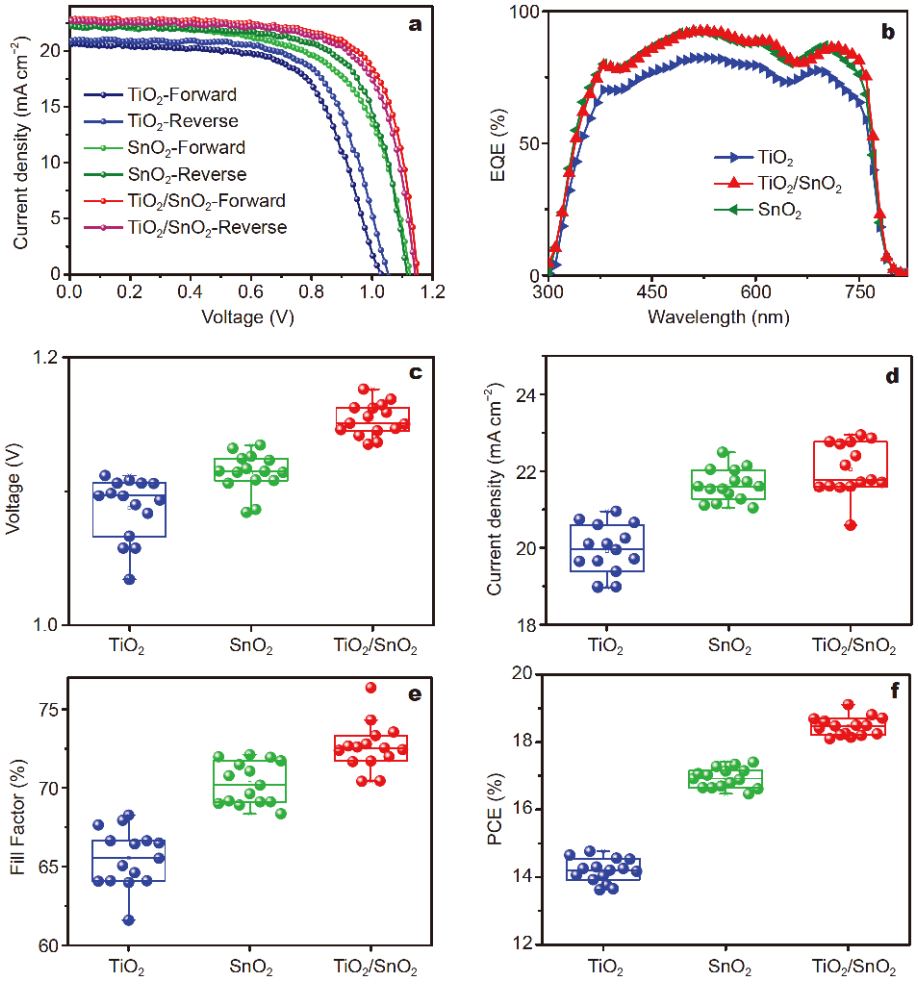

Figure 4 The *J-V* (a) and EQE curves (b) of the champion devices with different ETLs and the box charts of the PSCs with the different ETLs (c–f), the number of total samples accounted for statistics is 45.

Table 1 The photovoltaic statistical data of the PSCs based on the different ETLs (45 PSCs)

Samples	V_{oc} (V)	J_{sc} (mA cm^{-2})	FF (%)	PCE (%)
TiO_2	1.09 (± 0.02)	19.92 (± 0.65)	65.54 (± 1.84)	14.18 (± 0.35)
SnO_2	1.11 (± 0.01)	21.63 (± 0.42)	70.24 (± 1.34)	16.92 (± 0.29)
TiO_2/SnO_2	1.15 (± 0.01)	22.06 (± 0.67)	72.60 (± 1.46)	18.46 (± 0.27)

characteristics from the PSCs (total number of samples: 45 pieces of devices) based on the different ETLs, implying a great reproducibility of our devices. Obviously, the TiO_2/SnO_2-PSCs show the best performance compared with the TiO_2 and SnO_2-based devices. It is worth noting that the TiO_2/SnO_2 PSC shows the highest V_{oc} of 1.18 V (Fig. S5) and the average V_{oc} of 1.15 V, proving that this bilayer ETL fabricated at a low temperature is an effective way to improve V_{oc}. It is considered that the good conduction band alignment, excellent electron extraction and low recombination at the interface are the reasons for the amelioration of devices [36].

With the aim of further understanding the charge transfer and recombination kinetics in PSCs, dark *J-V* and EIS are performed. Fig. 5a shows the results in semilogarithmic plots of the dark *J-V* data, where the curves are in accordance with the Shockley diode equation:

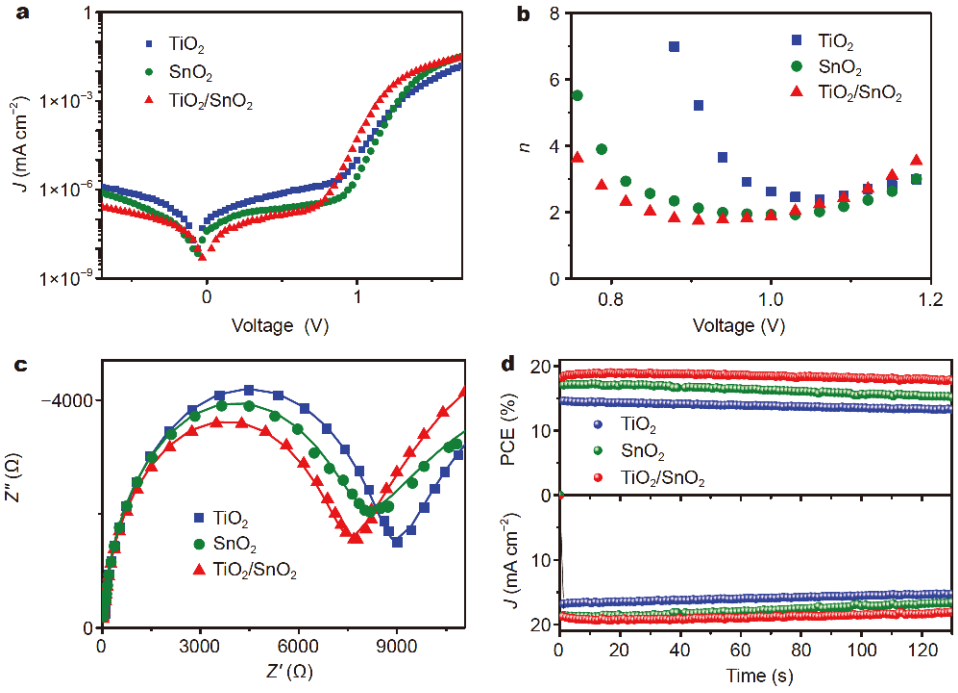

Figure 5 (a) The semi-logarithmic plots of the dark *J*-*V* curves, (b) the *n*-*V* curves, (c) the EIS spectra, and (d) the steady-state output performance of the same set of PSCs.

$$J = J_0\left[\exp\left(\frac{qV}{n\kappa T}\right) - 1\right], \tag{1}$$

where J_0 is the reverse saturation current density, T is the temperature in Kelvin, n is the ideality factor, and κ is the Boltzmann constant. Compared with the PSCs with single TiO_2 or SnO_2 ETLs, the PSCs with a TiO_2/SnO_2 bilayer ETL show lower J_0 values and inflection points, suggesting a more effective charge selective contact due to the lower charge recombination and leakage [37]. The n value is linked to the recombination upon the defect-state density, obtained from the differentiation of the Shockley diode equation [38]:

$$n = \left[\frac{\kappa T \partial \ln J}{q \partial V}\right]^{-1}. \tag{2}$$

The *n*-*V* curves are depicted in Fig. 5b, which are determined by the plateau within the range of 0.8 to 1.1 V, in keeping with the linear relationship in Fig. 5a. The actual n values are 2.38, 1.89 and 1.75 for the TiO_2, SnO_2 and TiO_2/SnO_2 PSCs, respectively, indicating that the trap-assisted recombination is efficiently suppressed at the interface of the TiO_2/SnO_2 layer and perovskites.

EIS is also an effective method for investigating the electric role of ETLs in the performance of PSCs. The EIS spectra and the equivalent circuit model are presented in Fig. 5c and Fig. S7, respectively, while Z-view software is used to fit the Nyquist plots with the fitting results listed in Table S2. The series resistance (R_s) in the equivalent circuits originates from the connecting wire and the direct current (DC) resistance of PSCs. The high frequency region is attributed to the charge transfer resistance (R_{tr}), while the low frequency region is determined by the recombination resistance (R_{rec}) [39]. It is believed that the structures of all the devices are supposed to be the same, except for the ETLs. Thus, R_{tr} and R_{rec} directly reflect the impact of the ETLs on the PSCs, of which the values are summarized in Table S2. The TiO_2/SnO_2 PSC has the smallest semicircle with the lowest R_{tr} value, giving rise to a higher FF, which possibly originated from the highest electron mobility and ability of charge extraction. Meanwhile, the higher R_{rec} of the TiO_2/SnO_2 PSC evidently decreases in the interfacial recombination, which will lead to an improvement in V_{oc} of the devices. These results are in accord with the TRPL measurement on the different ETLs. Fig. 5d displays the change in the current density and PCE over time, reflecting the output stability of the PSCs with the different ETLs. The static PCEs at the maximum power point are 18.83%, 17.26% and 14.54% for PSCs based on TiO_2/SnO_2, SnO_2, and TiO_2

ETLs, respectively, which are measured under bias voltages of 0.980, 0.917 and 0.871 V, respectively (the voltages at the maximum power point in the *J-V* curves). Therefore, the TiO_2/SnO_2 PSC displays the most stable power output compared with other PSCs with monolayer ETLs.

CONCLUSIONS

In summary, a low-temperature process is adopted to prepare TiO_2/SnO_2 bilayer ETLs, which display superior electrical properties. The characterization results give direct evidence that the TiO_2/SnO_2 bilayer ETL improves the electron extraction and transport properties and adjusts the band alignment between the ETL and perovskite layers. Consequently, the TiO_2/SnO_2 PSCs achieve the highest V_{oc} of 1.18 V, which is much better than that of the TiO_2 or SnO_2 PSCs. The champion TiO_2/SnO_2 PSC is achieved with a PCE of 19.11%, a V_{oc} of 1.15 V, a J_{sc} of 22.77 mA cm^{-2}, and an FF of 72.38%. It is demonstrated that the TiO_2/SnO_2 film annealed at a low temperature is a prospective substitute ETL for conventional high-temperature sintered ETLs, as well as for fabricating flexible PSCs and tandem solar cells.

Received 3 July 2019; accepted 18 August 2019; published online 18 September 2019

1 Kojima A, Teshima K, Shirai Y, *et al.* Organometal halide perovskites as visible-light sensitizers for photovoltaic cells. J Am Chem Soc, 2009, 131: 6050–6051
2 Lee MM, Teuscher J, Miyasaka T, *et al.* Efficient hybrid solar cells based on meso-superstructured organometal halide perovskites. Science, 2012, 338: 643–647
3 Yang WS, Park BW, Jung EH, *et al.* Iodide management in formamidinium-lead-halide–based perovskite layers for efficient solar cells. Science, 2017, 356: 1376–1379
4 Jiang Q, Zhao Y, Zhang X, *et al.* Surface passivation of perovskite film for efficient solar cells. Nat Photon, 2019, 13: 460–466
5 Ma S, Cai M, Cheng T, *et al.* Two-dimensional organic-inorganic hybrid perovskite: from material properties to device applications. Sci China Mater, 2018, 61: 1257–1277
6 Xing G, Mathews N, Sun S, *et al.* Long-range balanced electron- and hole-transport lengths in organic-inorganic $CH_3NH_3PbI_3$. Science, 2013, 342: 344–347
7 Liu Y, Yang Z, Cui D, *et al.* Two-inch-sized perovskite $CH_3NH_3PbX_3$ (X = Cl, Br, I) crystals: Growth and characterization. Adv Mater, 2015, 27: 5176–5183
8 Chen H, Ye F, Tang W, *et al.* A solvent- and vacuum-free route to large-area perovskite films for efficient solar modules. Nature, 2017, 550: 92–95
9 Manser JS, Kamat PV. Band filling with free charge carriers in organometal halide perovskites. Nat Photon, 2014, 8: 737–743
10 Mahmood K, Sarwar S, Mehran MT. Current status of electron transport layers in perovskite solar cells: materials and properties. RSC Adv, 2017, 7: 17044–17062
11 Calió L, Kazim S, Grätzel M, *et al.* Hole-transport materials for perovskite solar cells. Angew Chem Int Ed, 2016, 55: 14522–14545
12 Yang G, Tao H, Qin P, *et al.* Recent progress in electron transport layers for efficient perovskite solar cells. J Mater Chem A, 2016, 4: 3970–3990
13 Jiang C, Lim SL, Goh WP, *et al.* Improvement of $CH_3NH_3PbI_3$ formation for efficient and better reproducible mesoscopic perovskite solar cells. ACS Appl Mater Interfaces, 2015, 7: 24726–24732
14 Rong Y, Hou X, Hu Y, *et al.* Synergy of ammonium chloride and moisture on perovskite crystallization for efficient printable mesoscopic solar cells. Nat Commun, 2017, 8: 14555
15 Jiang Q, Chu Z, Wang P, *et al.* Planar-structure perovskite solar cells with efficiency beyond 21%. Adv Mater, 2017, 29: 1703852
16 Liu M, Johnston MB, Snaith HJ. Efficient planar heterojunction perovskite solar cells by vapour deposition. Nature, 2013, 501: 395–398
17 Chen CW, Kang HW, Hsiao SY, *et al.* Efficient and uniform planar-type perovskite solar cells by simple sequential vacuum deposition. Adv Mater, 2014, 26: 6647–6652
18 Li Y, Cooper JK, Liu W, *et al.* Defective TiO_2 with high photoconductive gain for efficient and stable planar heterojunction perovskite solar cells. Nat Commun, 2016, 7: 12446
19 Shalan AE, Narra S, Oshikiri T, *et al.* Optimization of a compact layer of TiO_2 *via* atomic-layer deposition for high-performance perovskite solar cells. Sustain Energy Fuels, 2017, 1: 1533–1540
20 Conings B, Baeten L, Jacobs T, *et al.* An easy-to-fabricate low-temperature TiO_2 electron collection layer for high efficiency planar heterojunction perovskite solar cells. APL Mater, 2014, 2: 081505
21 Liu Z, Chen Q, Hong Z, *et al.* Low-temperature TiO_x compact layer for planar heterojunction perovskite solar cells. ACS Appl Mater Interfaces, 2016, 8: 11076–11083
22 Hu W, Zhou W, Lei X, *et al.* Low-temperature *in situ* amino functionalization of TiO_2 nanoparticles sharpens electron management achieving over 21% efficient planar perovskite solar cells. Adv Mater, 2019, 31: 1806095
23 Liu X, Wu Z, Zhang Y, *et al.* Low temperature Zn-doped TiO_2 as electron transport layer for 19% efficient planar perovskite solar cells. Appl Surf Sci, 2019, 471: 28–35
24 Unger EL, Hoke ET, Bailie CD, *et al.* Hysteresis and transient behavior in current–voltage measurements of hybrid-perovskite absorber solar cells. Energy Environ Sci, 2014, 7: 3690–3698
25 Chueh CC, Li CZ, Jen AKY. Recent progress and perspective in solution-processed interfacial materials for efficient and stable polymer and organometal perovskite solar cells. Energy Environ Sci, 2015, 8: 1160–1189
26 Wojciechowski K, Stranks SD, Abate A, *et al.* Heterojunction modification for highly efficient organic–inorganic perovskite solar cells. ACS Nano, 2014, 8: 12701–12709
27 Tan H, Jain A, Voznyy O, *et al.* Efficient and stable solution-processed planar perovskite solar cells *via* contact passivation. Science, 2017, 355: 722–726
28 Anaraki EH, Kermanpur A, Steier L, *et al.* Highly efficient and stable planar perovskite solar cells by solution-processed tin oxide. Energy Environ Sci, 2016, 9: 3128–3134
29 Jiang Q, Zhang L, Wang H, *et al.* Enhanced electron extraction using SnO_2 for high-efficiency planar-structure $HC(NH_2)_2PbI_3$-based perovskite solar cells. Nat Energy, 2017, 2: 16177
30 Jiang E, Yan J, Ai Y, *et al.* Defect engineering of oxygen vacancies

in SnO_x electron transporting layer for perovskite solar cells. Mater Today Energy, 2019, 12: 389–397
31 Song S, Kang G, Pyeon L, *et al.* Systematically optimized bilayered electron transport layer for highly efficient planar perovskite solar cells (η = 21.1%). ACS Energy Lett, 2017, 2: 2667–2673
32 Tavakoli MM, Yadav P, Tavakoli R, *et al.* Surface engineering of TiO_2 ETL for highly efficient and hysteresis-less planar perovskite solar cell (21.4%) with enhanced open-circuit voltage and stability. Adv Energy Mater, 2018, 8: 1800794
33 Li Y, Meng L, Yang YM, *et al.* High-efficiency robust perovskite solar cells on ultrathin flexible substrates. Nat Commun, 2016, 7: 10214
34 Yang D, Zhou X, Yang R, *et al.* Surface optimization to eliminate hysteresis for record efficiency planar perovskite solar cells. Energy Environ Sci, 2016, 9: 3071–3078
35 Reyna Y, Salado M, Kazim S, *et al.* Performance and stability of mixed $FAPbI_3(0.85)MAPbBr_3(0.15)$ halide perovskite solar cells under outdoor conditions and the effect of low light irradiation. Nano Energy, 2016, 30: 570–579
36 Correa Baena JP, Steier L, Tress W, *et al.* Highly efficient planar perovskite solar cells through band alignment engineering. Energy Environ Sci, 2015, 8: 2928–2934
37 Wang Q, Shao Y, Dong Q, *et al.* Large fill-factor bilayer iodine perovskite solar cells fabricated by a low-temperature solution-process. Energy Environ Sci, 2014, 7: 2359–2365
38 Wetzelaer GJAH, Scheepers M, Sempere AM, *et al.* Trap-assisted non-radiative recombination in organic-inorganic perovskite solar cells. Adv Mater, 2015, 27: 1837–1841
39 Huang X, Hu Z, Xu J, *et al.* Low-temperature processed SnO_2 compact layer by incorporating TiO_2 layer toward efficient planar heterojunction perovskite solar cells. Sol Energy Mater Sol Cells, 2017, 164: 87–92

Acknowledgements This work was supported by the National Key Research and Development of China (2018YFB1500103 and 2018YFB0704100), the National Natural Science Foundation of China (61574145, 61874177, 51502315 and 61704176), Zhejiang Provincial Natural Science Foundation (LR16F040002), Zhejiang Energy Group (znkj-2018-118).

Author contributions Ye J designed and engineered the experiments; Li N and Ai Y performed the experiments; Li N and Yan J conceived the fabrication process of the device; Li N and Jiang E performed the data analysis; Li N and Sheng J wrote the paper with the support from Yan B; Shou C and Lin L contributed to the theoretical analysis. All authors contributed to the general discussion.

Conflict of interest The authors declare that they have no conflict of interest.

Supplementary information Experimental details and supporting data are available in the online version of the paper.

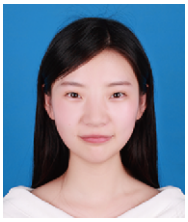

Nan Li is a joint training MSc student in Ningbo Institute of Materials Technology and Engineering (NIMTE), Chinese Academy of Sciences (CAS), supervised by Prof. Jichun Ye. She received her BSc degree in new energy technology and engineering from Central South University, Changsha, China, in 2017. Her research interests focus on the interface engineering and carrier dynamic process for perovskite solar cells.

Jiang Sheng received his PhD degree in the Institute of Plasma Physics, Chinese Academy of Sciences, China, in 2012. After being a postdoctoral in NIMTE, CAS (2013–2015), he worked as an associate professor since then. His research mainly focuses on the nanomaterials, interface engineering and carrier dynamic process for perovskite solar cells, silicon heterojunction solar cells. He has published more than 40 peer-reviewed papers, and filed more than 10 patents.

Jichun Ye received PhD degree in materials science from the University of California, Davis, USA in 2005. He joined NIMTE, CAS, as a professor and PhD advisor since August of 2012. He was awarded for "Thousand Young Talents Program of China" in 2012. He has published more than 60 peer-reviewed papers with nearly 500 citations, and filed more than 40 patents (including 10 awarded patents).

低温TiO_2/SnO_2双电子传输层的光电性能及其在钙钛矿电池中的应用

李楠[1,2], 闫锦[1,2], 艾余钱[1], 姜二帅[1,2], 林鎏金[1], 寿春晖[3], 闫宝杰[1], 盛江[1*], 叶继春[1,2*]

摘要 作为有机-无机钙钛矿杂化太阳能电池(PSCs)常用的电子传输层(ETL), 氧化钛(TiO_2)须在高温下烧结才能结晶, 因而难以适用于柔性和串联叠层太阳能电池. 本文介绍了一种低温溶液法制备TiO_2/氧化锡(SnO_2)电子传输层, 并通过对TiO_2/SnO_2 ETL的系统光学和电学性能测试, 证明TiO_2/SnO_2 ETL与钙钛矿层界面之间具有更好的电荷抽取能力和较少的载流子复合, 这有利于光致载流子的分离和传输. 因此, 与单一的ETL相比, 基于TiO_2/SnO_2的PSCs展现出更好的光伏性能, 其最大光电转换效率(PCE)为19.11%, 开路电压(V_{oc})为1.15 V, 短路电流密度为22.77 mA cm^{-2}, 填充因子为72.38%. 此外, 由于TiO_2/SnO_2电子传输层与钙钛矿层能带更匹配, 电池的V_{oc}最高达到了1.18 V. 综上所述, 本文提出了一种具有广泛应用前景的TiO_2/SnO_2电子传输层.

